

THERMAL STUDY OF OCTYLCYANOBIPHENYL LIQUID CRYSTAL CONFINED TO CONTROLLED-PORE GLASS¹

Z. Kutnjak^{2,5}, S.Kralj^{2,3}, G. Lahajnar^{2,4} and S. Žumer^{2,4}

¹ Paper presented at the Fifteenth Symposium on Thermophysical Properties, June 22-27, 2003, Boulder, Colorado, U.S.A.

² Condensed Matter Physics Department, Jozef Stefan Institute, P.O. Box 3000, 1000 Ljubljana, Slovenia

³ Laboratory of Physics of Complex Systems, Faculty of Education, University of Maribor, Koroska 160, 2000 Maribor, Slovenia

⁴ Department of Physics, Faculty of Mathematics and Physics, University of Ljubljana, Jadranska 19, 1000 Ljubljana, Slovenia

⁵ To whom correspondence should be addressed. E-mail: zdravko.kutnjak@ijs.si

ABSTRACT

We study the phase behavior of octylcyanobiphenyl (8CB) liquid crystal confined to control porous glass (CPG) using high resolution calorimetry. We used silanized and nonsilanized CPG matrices with characteristic void diameters ranging from 400 to 20 nm. With decreasing diameter the first order isotropic to nematic (I-N) and second order nematic to smectic A (N-SmA) phase transition temperatures monotonously decrease. The weakly first-order features of the I-N transition approaches the smeared tricritical behavior. The effective N-SmA critical exponent apparently decreases toward the 3DXY value for diameters above 100 nm, however, the N-SmA transition progressively broadens and become strongly suppressed for diameters below 100 nm. A simple phenomenological model is used for a qualitative explanation of results.

KEY WORDS: controlled-pore glass; heat capacity; liquid crystal; nematic; octylcyanobiphenyl; phase transition; smectic.

1. INTRODUCTION

The liquid crystals (LC) confined to various porous matrices or LCs filled with inclusions [1-5] represent natural choice to study experimentally the effects of confinement and disorder on phase behavior of LC. Controlled-pore glasses (CPGs), aerogels and aerosils are often used. The CPGs matrices [6-7] consist of strongly connected nearly cylindrical voids of nearly monodispersed pore diameter distribution. In aerogels [3,8-10] voids are separated by randomly interconnected silica strands and

the size of voids is strongly irregular. As inclusions spherular aerosil particles [5,11] in most cases form a responsive grid, which can rearrange for strong enough elastic distortions imposed by a hosting LC phase. In these systems the degree of confinement and disorder can be controlled by changing the typical void diameter (CPG, aerogels) or changing the concentration of aerosil particles. In general the influence of disorder is the weakest for aerosils, intermediate for CPGs and the strongest in aerogels.

Calorimetric methods are particularly adequate to determine the character of liquid crystalline phase transitions in such confinements. The aerogel [3,8-10] and aerosil [5,11] systems have already been studied in detail. In this contribution we perform high-resolution calorimetric study of octylcyanobiphenyl (8CB) LC confined to nonsilanized and silanized CPGs with different characteristic void diameters. We discuss the results within the simple phenomenological model.

2. MEASUREMENTS

2.1. Specimens

We used CPG matrices with average pore diameters 395, 127.3, 72.9, 60, and 23.7 nm. A typical SEM photograph shown in Figures 1a and 1b indicates that CPG voids are strongly interconnected. The nonsilanized surface of voids is smooth down to the nanometer scale and is believed to enforce isotropic tangential anchoring (i.e. the molecules tend to lie in any direction perpendicular to a void's surface normal) to most LCs [12].

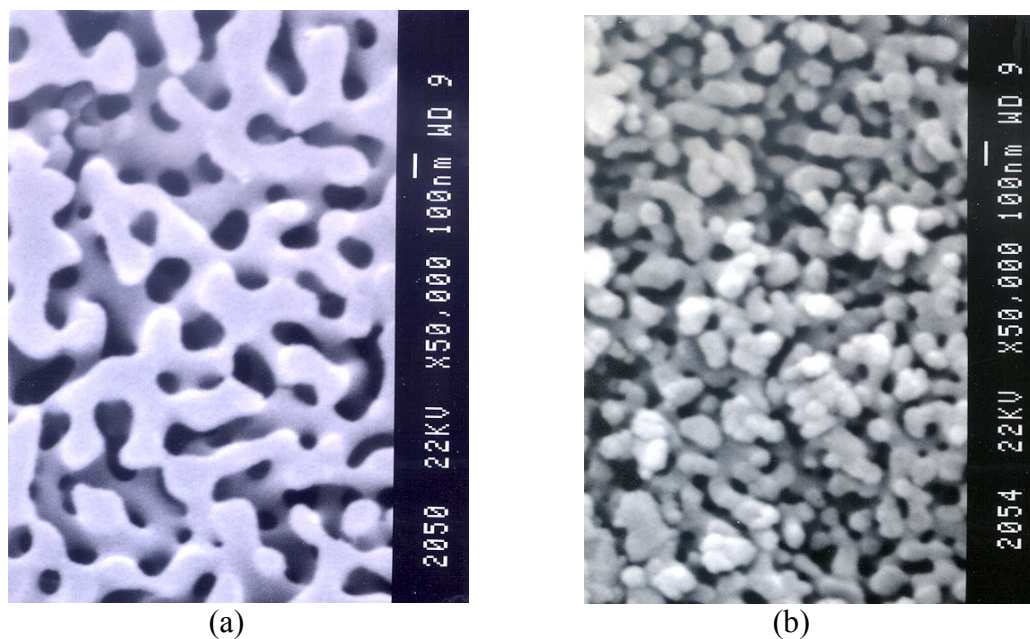


Fig. 1. (a) The SEM photograph of an empty controlled-pore glass matrix of $2R=127.3$ nm and (b) $2R\sim 60$ nm.

In order to enhance the surface anchoring effects some CPG matrices were silanized. The nonsilanized and silanized matrices were filled in vacuum with octylcyanobiphenyl (8CB) liquid crystal. Bulk 8CB exhibits weakly first order Isotropic-Nematic (I-N), and nearly continuous Nematic-Smectic A (N-SmA) phase transition.

2.2. Experimental procedure

Heat-capacity data were taken by a computerized calorimeter. Description of the technique was extensively given in [13]. The calorimeter is capable of automated operation in either ac or relaxation modes in a temperature range from 80 K to 470 K. The sample contained in a sealed silver cell, is thermally linked to a temperature-stabilized bath by support wires and by air. The thermal link can be represented by a thermal resistivity $R_T \sim 250$.

In the ac mode, an oscillating heat $P_{ac}e^{i\omega t}$ with the frequency of $\omega=0.0767\text{s}^{-1}$ is supplied to the sample by a thin resistive heater. The temperature oscillations $T_{ac}=P_{ac}/(1/R_T+i\omega C)$ of the sample were detected by the small bead thermistor. Due to the anomalous response the ac mode does not provide quantitative value of the latent heat in the case of the first-order transition, however, the phase shift Φ of T_{ac} can be useful in discriminating between the first and second order phase transitions [13].

The data were taken on cooling the sample from Isotropic phase with the cooling rates between 100 mK/h to 300 mK/h. The typical amplitude of T_{ac} were between 10 mK to 20 mK. The mass of the sample was around 40 mg. Here typically around 50% of mass was due to CPG matrices. The heat capacities of empty CPG samples and the empty cell were later subtracted from the C_p data.

In the relaxation mode the heater power supplied to the cell is linearly ramped [13]. The effective heat capacity is calculated from $C_{eff}(T) = dH/dT = [P-(T-T_B)/R]/(dT/dt)$, where $R=(T(\infty)-T_B)/P_0$ and P is the power at some time $0 \leq t \leq t_1$ corresponding to sample temperature T between the bath temperature T_B and $T(\infty)$. Here typically $t_1 \sim 480$ s during which about 1500 sample temperature $T(t)$ data points were taken. Sample temperature heating/cooling rate dT/dt is calculated over a short time interval centered at t . The relaxation-mode data have slightly lower signal to noise ratio in comparison to the ac mode, however, the advantage of this mode, known also as nonadiabatic scanning mode, is much better sensitivity to latent heat than the ac mode. The total enthalpy is calculated as $H=\int C_{eff}dT$. The typical heating/cooling rate of $dT/dt \sim 7.5$ K/h was used in the relaxation mode and the typical ramping steps $T(\infty)-T_B$ were about 1 K.

3. RESULTS

Figures 2 and 3 show temperature dependence of the ac specific heat C_p across the I-N and N-SmA transitions for 8CB in nonsilanized and silanized CPG samples. A bulk 8CB reference sample has also been measured. The phase transition temperatures for bulk 8CB $T_{IN}=313.67$ K and $T_{NA}=306.71$ K were found to be in reasonable agreement with previously published values ranging from 306.598 K to 307.02 K for N-SmA transition and 313.60 K to 314.01 K [3,5,14,15]. The width of the Nematic temperature

range of 6.96 K and the 20 mK wide I-N phase coexistence region determined from slow ac runs agree very well with previous published values.

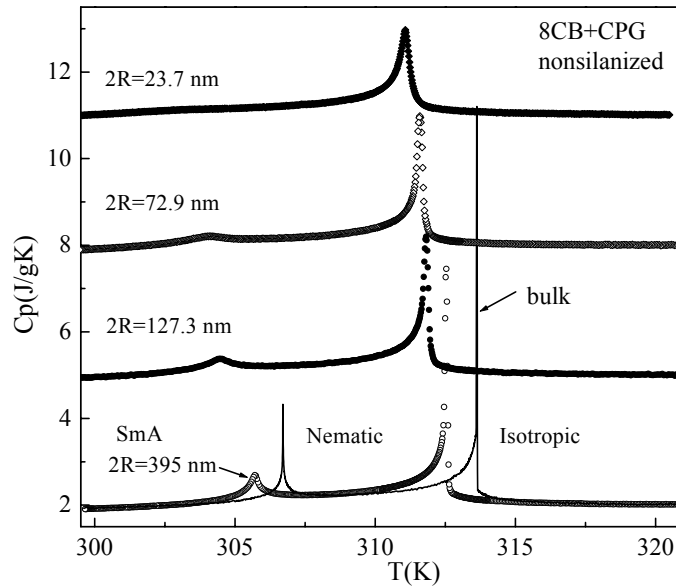


Fig. 2. Heat capacity C_p as a function of temperature for bulk 8CB and various nonsilanized CPG samples. The C_p data for $2R=127.3$ nm, 72.9 nm, and 23.7 nm were shifted by a constant background factor of 3, 6, and 9 J/gK.

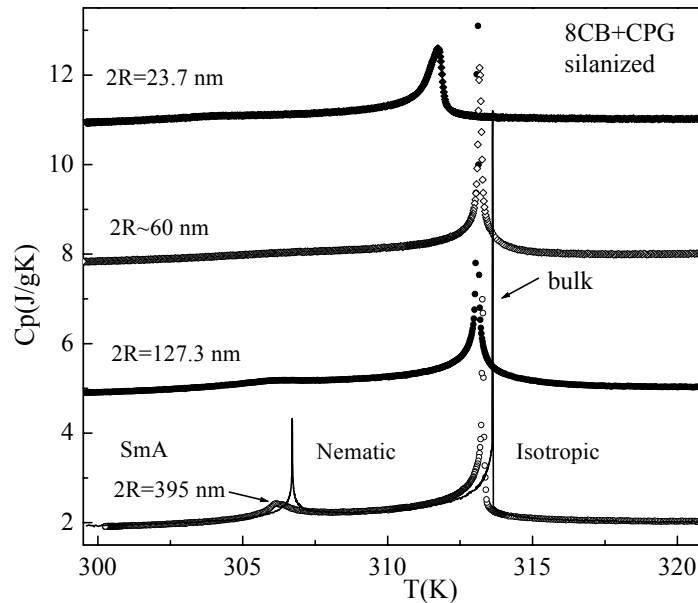


Fig. 3. Heat capacity C_p as a function of temperature for bulk 8CB and various silanized CPG samples. The C_p data for $2R=127.3$ nm, 60 nm, and 23.7 nm were shifted by a constant background factor of 3, 6, and 9 J/gK.

It is obvious from Figs. 2 and 3 that by decreasing the pore diameter both I-N and N-SmA transition temperatures are shifted considerably to lower temperatures and due to the significant rounding effects both anomalies are considerably suppressed.

Characteristic temperature shifts of the I-N and N-SmA transition temperatures with the respect to the bulk 8CB transition temperatures are given in Table I.

Table I. Phase transition temperature shifts for 8CB in controlled-pore glasses of various pore diameter $2R$. ΔT_{IN} and ΔT_{NA} represents shifts of I-N and N-SmA transitions, respectively. Also shown are width of the nematic phase ΔT_N , effective critical exponent α_{NA} , and the peak value of the excessive heat capacity C_p^{max} at the N-SmA transition. Phase transition temperatures for bulk 8CB: $T_{IN}=313.67$ K and $T_{NA}=306.71$ K. Silanized and nonsilanized samples are indicated by S and NS, respectively.

8CB+CPG's, 2R [nm]	ΔT_{IN} [K]	ΔT_{NA} [K]	ΔT_N [K]	α_{NA}	C_p^{max} [J/gK]
8CB bulk	0.00	0.00	6.96	0.27±0.03	2.224
S 395nm	0.34	0.43	7.00	0.09±0.05	0.351
S 127.3nm	0.52	0.64	7.03	0.06±0.10	0.121
S 60 nm	0.44	0.16	6.63	-	0.041
S 23.7nm	1.88	2.80	7.83	-	0.0379
NS 395nm	1.08	1.00	6.83	0.19±0.05	0.596
NS 127.3nm	1.80	2.25	7.36	0.10±0.08	0.297
NS 72.9nm	2.03	2.60	7.48	0.07±0.10	0.169
NS 23.7nm	2.55	3.76	8.12	0.04±0.15	0.033

Table II. Enthalpy changes of the I-N and N-SmA phase transitions for bulk 8CB and 8CB in CPGs of various pore diameter $2R$. $\Delta H_{IN}=\delta H_{IN} + L_{IN}$ is the total transition enthalpy of the I-N transition, δH_{IN} is the continuous contribution to the ΔH_{IN} and L_{IN} is the latent heat. ΔH_{NA} is the total transition enthalpy of N-SmA transition. Note that in case of bulk small difference was observed between ΔH_{NA} obtained from ac data and relaxation data most likely due to the small presence of latent heat. In CPG samples no latent heat was observed at N-SmA transition, thus only ac data are presented. Silanized and nonsilanized samples are indicated by S and NS, respectively.

8CB+CPG's, 2R [nm]	ΔH_{IN} [J/g]	δH_{IN} [J/g]	L_{IN} [J/g]	ΔH_{NA} [J/g]
8CB bulk	7.97±0.1	5.77±0.1	2.20±0.05	0.75±0.03 ^{ac} , 0.84±0.04 ^{rlx}
S 395nm	7.66±0.1	5.85±0.1	1.81±0.05	0.74±0.03 ^{ac}
S 127.3nm	7.68±0.1	6.43±0.1	1.25±0.05	0.52±0.03 ^{ac}
S 60 nm	7.50±0.1	6.59±0.1	0.91±0.05	0.20±0.02 ^{ac}
S 23.7nm	7.19±0.2	6.53±0.2	0.66±0.1	0.11±0.02 ^{ac}
NS 395nm	7.80±0.1	5.85±0.1	1.95±0.05	0.70±0.03 ^{ac}
NS 127.3nm	7.77±0.1	6.09±0.1	1.68±0.05	0.63±0.03 ^{ac}
NS 72.9nm	7.57±0.1	6.17±0.1	1.40±0.05	0.43±0.03 ^{ac}
NS 23.7nm	7.38±0.2	6.22±0.2	1.16±0.1	0.12±0.02 ^{ac}

^{ac}ac run data.

^{rlx}Nonadiabatic scanning (relaxation) run data.

Figure 4 shows the relaxation heat capacity data C_{eff} (open circles) and the ac data (solid line) obtained in the vicinity of the I-N (a) and N-SmA transition (b) for 8CB in CPG of pore diameter $2R=395$ nm. Significant difference in the size of the I-N anomaly between ac data (solid line in Fig. 4a) and relaxation data indicates presence of the latent heat L . Although the I-N latent heat decreases substantially its presence could be detected even for the CPG samples with the smallest pore diameter of 23.7 nm, (see Table II). Note the progressive smearing of the I-N phase transition with decreasing pore diameter. In the case of N-SmA anomaly (Fig. 4b) no difference was observed between the ac and relaxation data indicating absence of the latent heat.

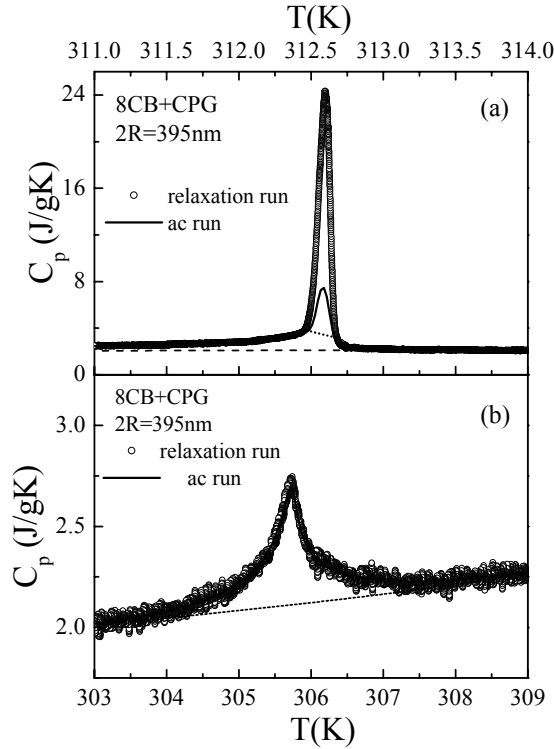


Fig. 4. (a) Heat capacity variations near the I-N transition obtained in a relaxation run (open circles) and in an ac run (solid line) for a nonsilanized CPG sample of $2R=395$ nm. The $C_p(background)$ expected in the absence of all transitions is represented by the dashed line. The dotted line represents the background above which the C_{eff} response is predominantly induced due to the presence of the latent heat. (b) C_p variations near the N-SmA transition obtained in a relaxation run (open circles) and in an ac run (solid line) for the same nonsilanized CPG sample of $2R=395$ nm. The dashed baseline represents I-N C_p wing expected in the absence of the N-SmA transition.

The Table II provides enthalpy changes of the I-N and N-SmA phase transitions for all samples. The total transition enthalpy ΔH for weakly first-order transitions is given by $\Delta H = \delta H + L$. Here, continuous variations of the enthalpy δH can be defined as integral of the excess heat capacity $\delta H = \int \Delta C_p dT$. The integration covers the entire heat capacity peak excluding the anomalous response due to the latent heat L within the coexistence range. For the second order transition $\Delta H = \delta H$. In principle δH can be obtained from both ac and relaxation runs, while L can be quantitatively deducted only from the relaxation run. The excess heat capacity associated with some particular

transition can be defined as $\Delta C_p = C_p(T) - C_p(\text{baseline})$, where $C_p(\text{baseline})$ represents C_p variations expected in the absence of a particular phase transition. For illustration regarding baselines see also Figs. 4a and 4b.

Figures 5a and 5b show evolution of the N-SmA C_p peak (open circles) from bulk 8CB to CPG sample of $2R=127.3$ nm. The size of the N-SmA anomaly $\Delta C_p(\text{max})$ given in last column in Table I shrinks dramatically with decreasing pore diameter. We carried the N-SmA critical exponent analysis using the usual power-law form

$$\Delta C_p(R) = A^\pm |r|^{-\alpha(R)} (1 + D^\pm |r|^{0.5}) + B_C, \quad (1)$$

where $r = (T - T_{NA}(R)) / T_{NA}(R)$. Effective critical exponent $\alpha(R)$ is given in Table I.

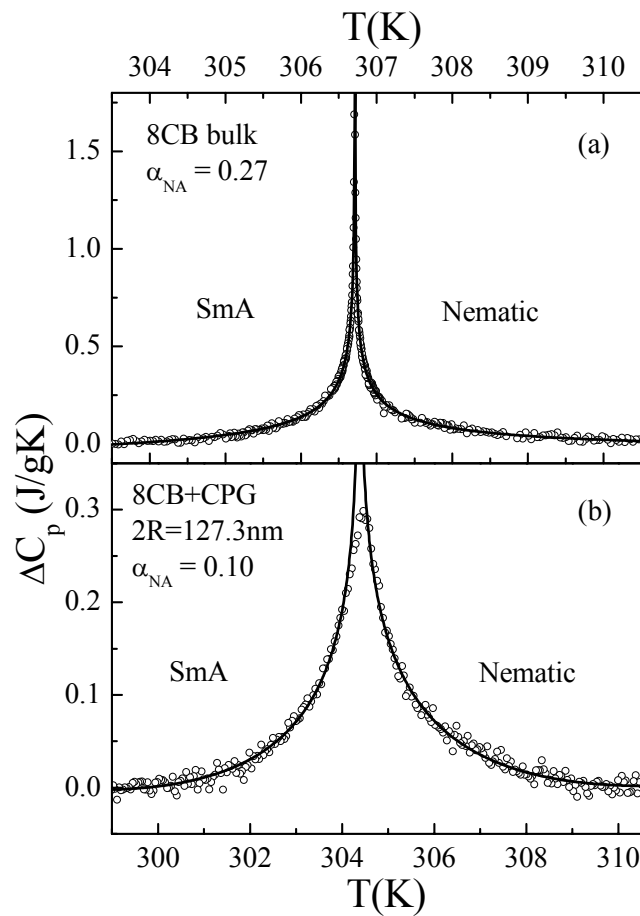


Fig. 5. Excess heat capacity near N-SmA transition. Solid line represents fits to the critical scaling ansatz (1).

By comparing the data in Figs. 2 and 3 it is possible to conclude that in the case of silanized samples the temperature shifts are less pronounced, N-SmA anomalies are more suppressed, and stronger I-N pretransitional C_p wing could be observed. Figure 6 shows comparison of C_p data for silanized and nonsilanized CPG samples near I-N and N-SmA transition. The strong I-N pretransitional wing induced by enhanced ordering effects imposed by the silanized surface could be observed for CPG sample of $2R=127.3$ nm (Fig. 6a). In the case of N-SmA transition the strong anchoring of the

silanized surface results rather in strong suppression and smearing of the N-SmA C_p anomaly (see Fig. 6b).

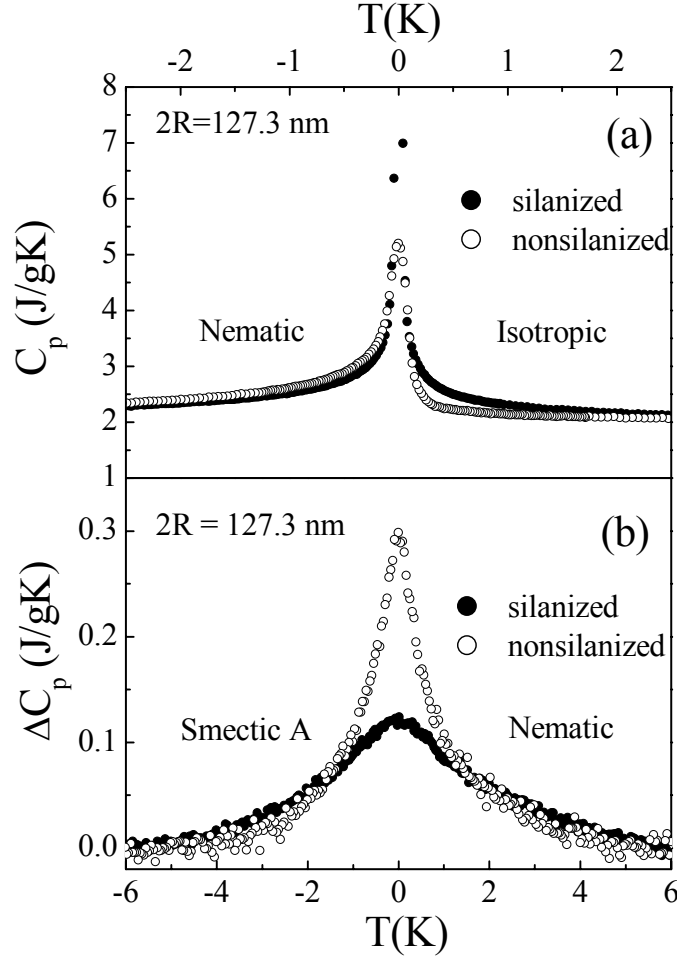


Fig. 6. (a) Comparison of $C_p(T)$ variations near I-N transition for nonsilanized (open circles) and silanized (solid circles) CPG samples of $2R=127.3$ nm. (b) Comparison of excess heat capacity temperature variations near NA transition for nonsilanized (open circles) and silanized (solid circles) CPG samples of $2R=127.3$ nm.

DISCUSSION

To explain the calorimetric results qualitatively we use Landau-de Gennes type phenomenological approach. Due to lack of space we focus only on nonsilanized data. More detailed description of the phenomenological model for both nonsilanized and silanized cases will be given elsewhere. The nematic ordering is described in terms of the nematic director field \vec{n} and the nematic uniaxial order parameter S . The SmA ordering is given by the complex order parameter $\psi = \eta e^{i\phi}$, where η is the translational order parameter and the phase ϕ determines the position of smectic layers. The relevant energy potential F is expressed as $F = \iiint f_V dV + \iint f_S dS$ where f_V and f_S determine

the ‘‘volume’’ and ‘‘surface’’ energy densities of the confined LC phase. The volume contribution $f_V = f_h^{(n)} + f_e^{(n)} + f_h^{(s)} + f_e^{(s)} + f_c$ is given as a sum of homogeneous (subscript h) and elastic (subscript e) contributions of nematic (superscript $^{(n)}$) and smectic (superscript $^{(s)}$) terms. Here the f_c contribution is describing the coupling between positional and orientational LC ordering. To the lowest approximation we express the density terms as [16]

$$\begin{aligned}
f_h^{(n)} &= a_0(T - T_*)S^2 - BS^3 + CS^4, \\
f_e^{(n)} &= 1/2L_0S^2|\nabla\bar{n}|^2 + 1/2L_1|\nabla S|^2, \\
f_h^{(s)} &= \alpha_0(T - T_{NA})|\psi|^2 + \beta|\psi|^4, \\
f_e^{(s)} &= C_{||}|\bar{n}\cdot\nabla - iq_0\psi|^2 + C_{\perp}|(\bar{n}\times\nabla)\psi|^2, \\
f_c &= -D_C S|\psi|^2.
\end{aligned} \tag{2}$$

Here a_0 , α_0 , B , C , β are the material constants, T_* is the supercooling temperature of the bulk isotropic phase, and T_{NA} the temperature of the 2nd order bulk N-SmA phase transition for $D_C=0$. In a typical LC material T_* is approximately 1K below the the bulk I-N phase transition temperature T_{IN} . L_0 and L_1 are the bare nematic elastic constants, $C_{||}$ and C_{\perp} are the smectic compressibility and bend elastic constant, D_C is the coupling constant between the smectic and nematic order parameters, and $d_0=2\pi/q_0$ determines the equilibrium smectic layer thickness in the SmA phase.

The free energy surface contribution f_S enforcing the isotropic planar anchoring is consisting of the nematic orientational anchoring term $f_o^{(n)}$, the nematic disordering $f_d^{(n)}$, and the smectic positional anchoring $f_p^{(s)}$ given by

$$\begin{aligned}
f_o^{(n)} &= -\frac{W_1 S}{2}(1 - (\bar{n}\cdot\bar{v})^2), \\
f_d^{(n)} &= \frac{W_2 S^2}{2}, \\
f_p^{(s)} &= \frac{W_p}{2}|\psi - \psi_s|^2.
\end{aligned} \tag{3}$$

Here W_1 , W_2 , and W_p measure the surface interaction strengths and \bar{v} is the local normal to a CPG confining surface. The W_1 term enforces isotropic tangential anchoring, the W_2 term mimics the disordering effect arising from random voids' interconnections, and the W_p contribution introduces the positional anchoring potential.

In order to express the relevant physical quantities we first estimate the average nematic and smectic order parameter of the sample within the single pore approximation, i.e. $|\nabla S| \sim S_b/\xi_n(T)$ and $|\nabla\eta| \sim \eta_b/\xi_s(T)$. Here S_b and η_b describe the bulk values of the order parameters and $\xi_n(T)$, $\xi_s(T)$ represent the nematic and smectic order parameter correlation lengths, respectively. The geometry of the average pore is given by the pore radius R and the domain length ξ_d , which measures an average distance between adjacent strongly elastically distorted states enforced by the CPG matrix geometry. By minimizing the average energy density $\langle f \rangle = \langle F \rangle / V$, where V is the void volume of the sample occupied by LC, the equilibrium average order parameters are obtained. The excess heat capacity could then be calculated by using the expression

$\Delta C_p = -T(a_0 \partial S^2 / \partial T + \alpha_0 \partial \eta^2 / \partial T)$. The latent heat $L_{IN}(R)$ at the I-N transition is given by $L_{IN}(R) = a_0 T_{IN}(R) (S_-^2 - S_+^2)$, where S_- and S_+ describe the nematic order parameter value just below and above the transition temperature $T_{IN}(R)$ in the CPG of radius R . The temperature shifts with the respect to the bulk value are given by

$$\Delta T_{IN}(R) = (T_{IN} - T_*) (\xi_n^2 / 2\xi_d^2 + \xi_n / R - \xi_n^2 / R d_e^{(1)} + \xi_n^2 / R d_e^{(2)} + t_{def}), \quad (4)$$

$$\Delta T_{NA}(R) = T_{NA}(d_\infty) [(d_\infty - d(R) + \xi_s^2 / \xi_d^2 + 2\xi_s / R) / (1 + d_\infty)]. \quad (5)$$

Here $\xi_n = \xi_n(T_{IN}) = (L / (a_0(T_{IN} - T_*)))^{1/2}$ is the nematic order parameter correlation length, $\xi_s = \xi_s(0) = C / (\alpha_0 T_{NA})$ is the smectic order parameter correlation length expressed at $T=0$, $d_e^{(1)} = W_1 / LS_0$ and $d_e^{(2)} = W_2 / L$ are the surface extrapolation lengths expressed at $T=T_{IN}$, t_{def} is the contribution due to the point defects, and d_∞ is the coupling constant in the bulk in which the transition takes place at $T_{NA}(d_\infty)$.

Our C_p measurements show that with decreasing value of R the I-N and N-SmA transition temperatures and L_{IN} monotonously decrease. Figure 7 shows that the simple model predictions qualitatively agree with the experimental results obtained on nonsilanized CPG samples.

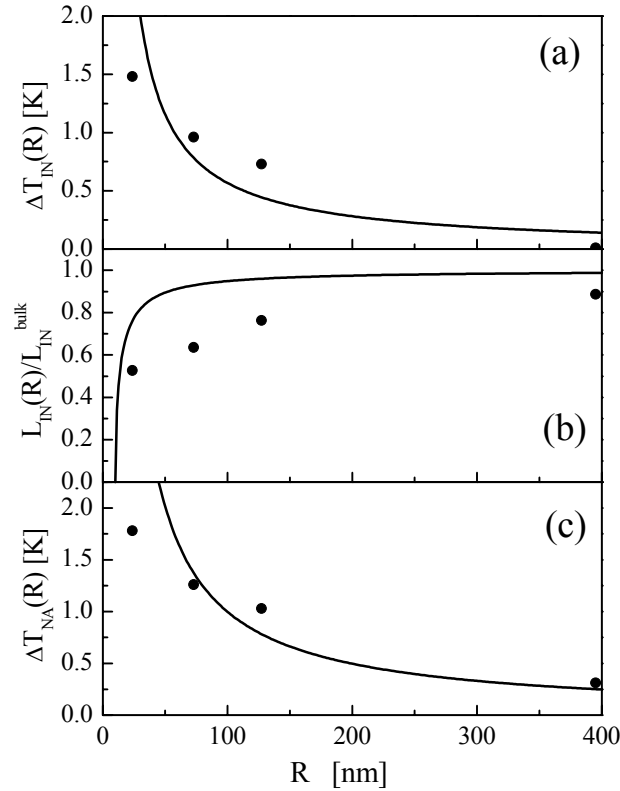


Fig. 7. (a) ΔT_{IN} , (b) Normalized latent heat, and (c) ΔT_{NA} as functions of pore radius R .

The decrease of transition temperature with increasing value of R can be in our rough description explained by ξ_n / ξ_d contribution. It describes the effective rise of the temperature (i.e. reduction of the transition temperature $T_{IN}(R)$) due to elastic distortions. Note that the predicted main cluster size ξ_d is expected to be proportional to

R . Therefore the Equation (4) suggests that the IN transition temperature shift is proportional to $1/R^2$. This elastic contribution in our samples dominates over the $1/R$ term, which tends to increase the transition temperature.

The N-SmA temperature shifts follows similar trend as for the I-N transition. Due to the tangential orientational anchoring condition we believe that the smectic layers grow along the cylindrically shaped voids. As in the nematic phase the sample then consists of domains of typical size $\xi_d \propto R$ that extend between adjacent defects. The dominant term affecting the temperature shift is the elastic contribution ($\propto (\xi_s/\xi_d)^2$), suggesting that the temperature shifts approximately scales as $1/R^2$. Note that the N-SmA transition is apparently more affected by confinement than the I-N transition. We believe that the main reason is randomness, which becomes increasingly important with decreasing value of R . The influence of randomness is more effective on the N-SmA than on the I-N transition since smectic correlation length exceeds the nematic one.

ACKNOWLEDGEMENTS

This research was supported by the ESF network project COSLAB, Slovene-Greek Cooperation project No. GR 20/2003, and Slovenian Office of Science.

REFERENCES

1. D.J. Cleaver, S. Kralj, T.J. Sluckin, and M.P. Allen, in *Liquid Crystals in Complex Geometries formed by polymer and porous networks*, G.P. Crawford, S. Žumer (eds.), Taylor and Francis, London, 1996, p. 467.
2. T. Bellini, L. Radzihovsky, J. Toner, and N. A. Clark, *Science*, 294 (2001) 1074.
3. T. Bellini, N. A. Clark, C. D. Muzny, L. Wu, C.W. Garland, D. W. Schaefer, and B. J. Oliver, *Phys. Rev. Lett.*, 69 (1992) 788.
4. G. S. Iannacchione and D. Finotello, *Phys. Rev. Lett.*, 69 (1992) 2094.
5. G. S. Iannacchione, C. W. Garland, J. T. Mang, and T. P. Rieker, *Phys. Rev. E*, 58 (1998) 5966.
6. M.D. Dadmun and M. Muthukumar, *J. Chem. Phys.*, 98 (1993) 4850.
7. S. Kralj, A. Zidanšek, G. Lahajner, S. Žumer, and R. Blinc, *Phys. Rev. E*, 57 (1998) 3021.
8. T. Bellini, N. A. Clark, and D. W. Schaefer, *Phys. Rev. Lett.*, 74 (1995) 2740.
9. L. Wu, B. Zhou, C.W. Garland, T. Bellini, and D.W. Schaefer, *Phys. Rev. E*, 51 (1995) 2157.
10. Z. Kutnjak and C.W. Garland, *Phys. Rev. E*, 55 (1997) 488.
11. Z. Kutnjak, S. Kralj, and S. Zumer, *Phys. Rev. E*, 66 (2002) 041702-1.
12. S. Kralj, A. Zidanšek, G. Lahajnar, I. Musevic, S. Zumer, R. Blinc, and M. Pinter, *Phys. Rev. E*, 53 (1996) 3629.
13. H. Yao and C.W. Garland, *Rev. Sci. Instrum.*, 69 (1998) 172.
14. G. B. Kasting, C. W. Garland, and K. J. Lushington, *J. Physique*, 41 (1980) 879.
15. J. Thoen, H. Marynissen, and W. Van Dael, *Phys. Rev. E*, 26 (1982) 2886.
16. S. Kralj and T. Sluckin, *Phys. Rev. E*, 50 (1994) 2940.